THE JOURNAL OF BIOLOGICAL CHEMISTRY VOL. 292, NO. 14, pp. 5695–5704, April 7, 2017

Covalently linked HslU hexamers support a probabilistic mechanism that links ATP hydrolysis to protein unfolding and translocation

Received for publication, November 21, 2016, and in revised form, February 7, 2017 Published, JBC Papers in Press, February 21, 2017, DOI 10.1074/jbc.M116.768978

Vladimir Baytshtok[‡], Jiejin Chen[‡1], Steven E. Glynn[‡2], Andrew R. Nager[‡3], Robert A. Grant[‡], Tania A. Baker[‡§], and Robert T. Sauer[‡4]

From the [‡]Department of Biology and [§]Howard Hughes Medical Institute, Massachusetts Institute of Technology, Cambridge, Massachusetts 02139

Edited by George N. DeMartino

The HslUV proteolytic machine consists of HslV, a double-ring self-compartmentalized peptidase, and one or two AAA+ HslU ring hexamers that hydrolyze ATP to power the unfolding of protein substrates and their translocation into the proteolytic chamber of HslV. Here, we use genetic tethering and disulfide bonding strategies to construct HslU pseudohexamers containing mixtures of ATPase active and inactive subunits at defined positions in the hexameric ring. Genetic tethering impairs HslV binding and degradation, even for pseudohexamers with six active subunits, but disulfide-linked pseudohexamers do not have these defects, indicating that the peptide tether interferes with HslV interactions. Importantly, pseudohexamers containing different patterns of hydrolytically active and inactive subunits retain the ability to unfold protein substrates and/or collaborate with HslV in their degradation, supporting a model in which ATP hydrolysis and linked mechanical function in the HslU ring operate by a probabilistic mechanism.

Enzymes of the AAA+ ATPase superfamily play roles in proteolysis, protein remodeling and disaggregation, replication, transcription, membrane fusion, vesicle transport, and other cellular processes in all organisms (1, 2). These enzymes share conserved sequence and structural motifs and typically function as homohexameric or heterohexameric rings. Fueled by the energy of ATP binding and hydrolysis, AAA+ enzymes act as molecular machines that disassemble, remodel, or denature macromolecule targets. There are three general models for how subunits in AAA+ hexamers hydrolyze ATP and generate the mechanical power strokes required for function: (i) concerted ATP hydrolysis that occurs simultaneously in all subunits (3); (ii) sequential hydrolysis by individual subunits that occurs in an invariant kinetic pattern (4); and (iii) probabilistic hydrolysis in which, following a power stroke, any ATP-bound subunit has some chance of hydrolyzing ATP to drive the next power stroke (5).

The HslUV protease consists of one or two AAA+ HslU hexamers and the dodecameric HslV peptidase (Fig. 1*A*) (6–12). In ATP-dependent reactions, HslU hexamers recognize protein substrates, unfold any native structure that is present, and then translocate the unfolded polypeptide into the luminal chamber of HslV for degradation. In all crystal structures of the *Escherichia coli* or *Haemophilus influenzae* HslUV complexes and some structures of HslU alone, the HslU hexamer is highly symmetric and binds six ATP or ADP molecules, as might be expected for a concerted mechanism of hydrolysis (6–12). However, in other structures of HslU alone, only three or four nucleotides are bound to the hexameric HslU ring (6), and solution experiments show detectable binding of a maximum of 3–4 nucleotides and the existence of at least two types of nucleotide-binding sites (13). These results suggest that the six subunits of HslU assume non-equivalent functional roles within the hexamer and are more consistent with sequential or probabilistic models. Here, we test different models by which ATP hydrolysis could power the mechanical functions of *E. coli* HslU by introducing hydrolytically inactive subunits at defined positions in its hexameric ring. Using subunit cross-linking strategies involving genetic tethering or disulfide bonding, we find that HslU pseudohexamers with mixtures of hydrolytically active and inactive subunits retain protein unfolding activity and support HslV degradation. These studies support a probabilistic mechanism in which ATP hydrolysis powers mechanical function in the HslU ring and also reveal new information about interactions between HslU and HslV.

Results

HslU dimers with covalent peptide tethers

HslU homohexamers containing the Walker B E257Q mutation are defective in ATP hydrolysis and protein degradation but retain the ability to bind HslV and protein substrates (13). We engineered genes to encode tandem *E. coli* HslU subunits

This work was supported by National Institutes of Health Grant AI-16892. The authors declare that they have no conflicts of interest with the contents of this article. The content is solely the responsibility of the authors and does not necessarily represent the official views of the National Institutes of Health.

The atomic coordinates and structure factors (code 5TXV) have been deposited in the Protein Data Bank (http://wwpdb.org/).

[1] Present address: Takeda Pharmaceuticals, Cambridge, MA 02139.

[2] Present address: Dept. of Biochemistry and Cell Biology, Stony Brook University, Stony Brook, NY 11794.

[3] Present address: Dept. of Molecular and Cellular Physiology, Stanford University, Stanford, CA 94305.

[4] To whom correspondence should be addressed. E-mail: bobsauer@mit.edu.

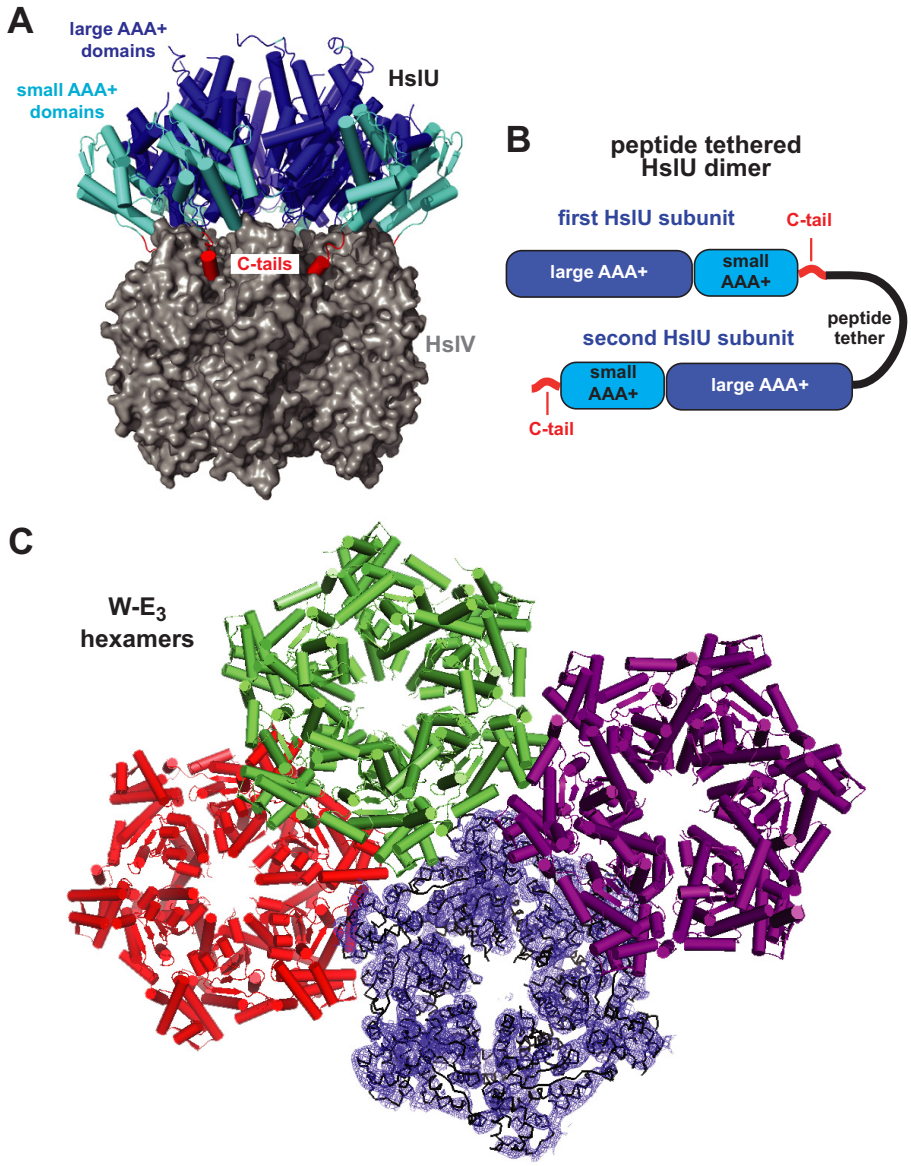

Figure 1. HslUV structure. *A*, an HslU hexamer (*secondary-structure representation*) bound to an HslV dodecamer (*surface representation*; Protein Data Bank code 1G3I). The large and small AAA+ domains of HslU and its C-terminal tails are colored *blue*, *cyan*, and *red*, respectively. *B*, tandem HslU subunits connected by a genetically encoded peptide tether. *C*, three W-E_3 hexamers in the asymmetric unit of structure 5TXV are shown in a *secondary-structure representation*; the fourth hexamer is shown in a *ribbon representation* with electron density from a composite omit map contoured at 1 σ.

connected by a 20-residue peptide tether (Fig. 1*B*). One encoded dimer consisted of two wild-type subunits (W-W), another had a wild-type subunit followed by an E257Q subunit (W-E), and a third had an E257Q subunit followed by a wild-type subunit (E-W). These dimers behaved like wild-type HslU during purification, suggesting that they form W-W_3, W-E_3, and E-W_3 pseudohexamers. Indeed, the asymmetric unit of a low-resolution W-E_3 crystal structure contained four hexamers similar to wild-type HslU (Fig. 1*C* and Table 1), although electron density for the C-terminal 8–10 residues was missing in alternating subunits of several hexamers or was generally poor throughout a hexamer, as expected if the tether disrupts normal C-terminal contacts.

W-W_3 hydrolyzed ATP at about twice the rate of the W-E_3 and E-W_3 enzymes (Fig. 2*A*), suggesting that ATP hydrolysis is largely restricted to the W subunits in these enzymes. We constructed and expressed a W-W-W trimer, but this protein was insoluble. To assay protein unfolding, we constructed an ^{I37A}Arc-^{cp6}GFP-st11-ssrA fusion protein with a thrombin cleavage site located between β-strands 5 and 6 (14). ^{I37A}Arc is a denatured variant of Arc repressor that targets the substrate to HslU, and the C-terminal st11-ssrA sequence increases the substrate turnover rate ~2-fold (15, 16). Following thrombin cleavage, unfolding of the split substrate by wild-type HslU results in an irreversible loss of GFP fluorescence. In experiments performed at different concentrations of the split substrate, unfolding by wild-type HslU and W-W_3 occurred with steady-state V_{max} rates that were similar, whereas V_{max} for unfolding by the W-E_3 and E-W_3 pseudohexamers was about half of the wild-type value (Fig. 2*B*). Thus, pseudohexamers with alternating ATPase active and inactive subunits retain substantial protein-unfolding activity. However, compared

with wild-type HslU, W-W_3 supported HslV degradation very poorly (Fig. 2*C*) and bound HslV ~20-fold more weakly (Table 2), probably because the peptide tether interferes with contacts between HslU and HslV (see "Discussion"). Thus, we explored a different method of constructing covalently linked HslU hexamers.

Construction of disulfide-cross-linked HslU pseudohexamers

HslU hexamers consist of rigid body units formed by the large and small domains of adjacent subunits (17). We used the Disulfide by Design algorithm (18) to identify Glu^{47}/Ala^{349} and Gln^{39}/Thr^{361} as sites for potential disulfide bonds across the rigid body interfaces of an HslU hexamer. Fig. 3*A* shows a model of an otherwise Cys-free HslU pseudohexamer in which *red* subunits contain Cys^{47} and *blue* subunits contain Cys^{349}, potentially allowing formation of three disulfide-linked dimers. To make $W^{SS}W_3$ pseudohexamers, the Cys^{47} and Cys^{349} subunits both had wild-type Walker B ATPase motifs. To make $W^{SS}E_3$ pseudohexamers, the Cys^{47} subunit had a wild-type Walker B sequence, and the Cys^{349} subunit contained the Walker B E257Q mutation to inactivate ATP hydrolysis. Fig. 3*B* shows a pseudohexamer in which *red* subunits contain Cys^{349}, *green* subunits contain Cys^{47} and Cys^{361}, and *blue* subunits contain Cys^{39}. In this configuration, formation of disulfide-linked trimers is possible. We designed $W^{SS}W^{SS}W$ trimers, $W^{SS}E^{SS}W$ trimers, and $W^{SS}E^{SS}E$ trimers by changing which subunits had wild-type or E257Q Walker B sites.

Relatively efficient formation of disulfide-linked HslU dimers or trimers was achieved by cytosolic coexpression of appropriate variants in the oxidizing SHuffle strain of *E. coli*

Table 1
Crystallographic statistics
Values in parenthesis represent the highest resolution shell.

Protein Data Bank code	5TXV
Wavelength (Å)	0.979
Space group	P 1 2_1 1
Unit-cell dimensions (Å)	$a = 86.5$; $b = 420.9$; $c = 176.5$
Unit-cell angles (degrees)	$\alpha = \gamma = 90$; $\beta = 98.6$
Resolution range (Å)	49.2–7.1 (7.3–7.1)
Unique reflections	18,630 (1784)
Completeness (%)	98.3 (94.6)
Redundancy	4.5 (4.5)
R_{merge}	0.105 (0.694)
R_{meas}	0.119 (0.782)
R_{pim}	0.055 (0.315)
R_{work}	0.274 (0.356)
R_{free}	0.298 (0.347)
MolProbity score (percentile)	100
Root mean square bonds (Å)	0.003
Root mean square angles (degrees)	0.61
Clash score	5.8
Favored rotamers (%)	99.0
Poor rotamers (%)	0.39
Ramachandran favored	98.0
Ramachandran outliers (%)	0
Bad bonds/angles	0/1
$C\beta$ deviations	0

Table 2
HslV binding
Titration assays, monitored by changes in HslV peptidase activity, were performed at 25 °C in the presence of 5 mM ATP.

Protein	$K_{1/2}$
	*n*M
Wild-type HslU	78 ± 11
W-W_3	1603 ± 278
$W^{SS}W_3$	59 ± 9
$W^{SS}W^{SS}W_2$	56 ± 5
$W^{SS}E^{SS}W_2$	21 ± 7
$W^{SS}E_3$	23 ± 11
$W^{SS}E^{SS}E_3$	28 ± 19

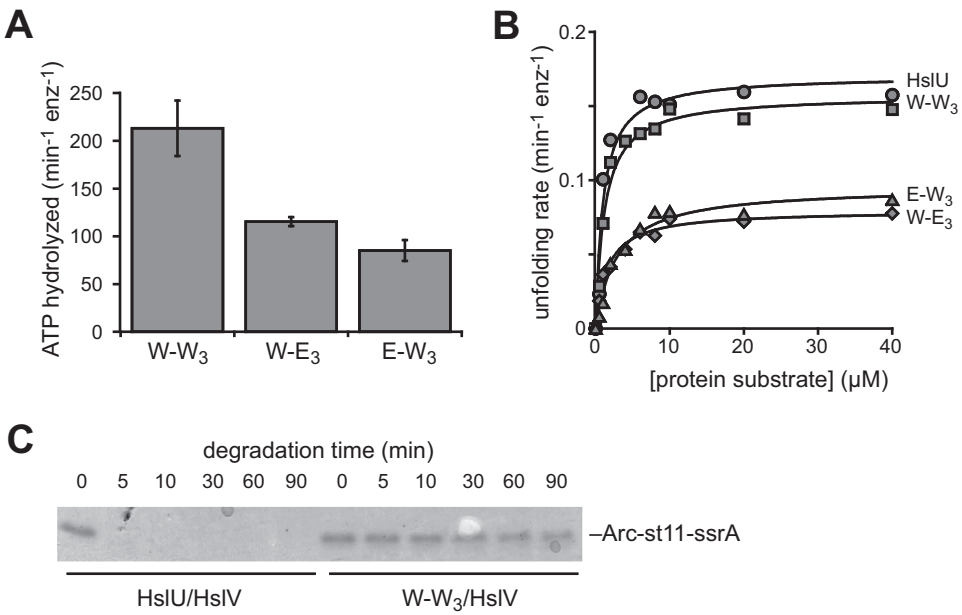

Figure 2. Activity of genetically tethered pseudohexamers. *A*, rates of hydrolysis of 5 mM ATP by the genetically tethered W-W_3, W-E_3, and E-W_3 pseudohexamers. Values are averages ($n \geq 5$) ± S.D. (*error bars*). *B*, rates of unfolding of different concentrations of thrombin-split ^{I37A}Arc-^{cp6}GFP-β5/β6-st11-ssrA by wild-type HslU or genetically tethered variants. *Lines*, non-linear least squares fits to the Michaelis-Menten equation. K_m values for all enzymes were 1–3 μM but were not well determined because of the small number of low-concentration data points. Average V_{max} values ± S.D. calculated from the highest four substrate concentrations were 0.155 ± 0.003 min^{-1} enz^{-1} (HslU), 0.143 ± 0.008 min^{-1} enz^{-1} (W-W_3), 0.0802 ± 0.007 min^{-1} enz^{-1} (E-W_3), and 0.0716 ± 0.006 min^{-1} enz^{-1} (W-E_3). Fitted V_{max} values were 10–15% higher. *C*, the kinetics of degradation of Arc-st11-ssrA (10 μM) by HslV (10 μM) and HslU (0.3 μM) or W-W_3 (0.3 μM) at 50 °C was monitored by SDS-PAGE. Reactions contained 5 mM ATP and a regeneration system.

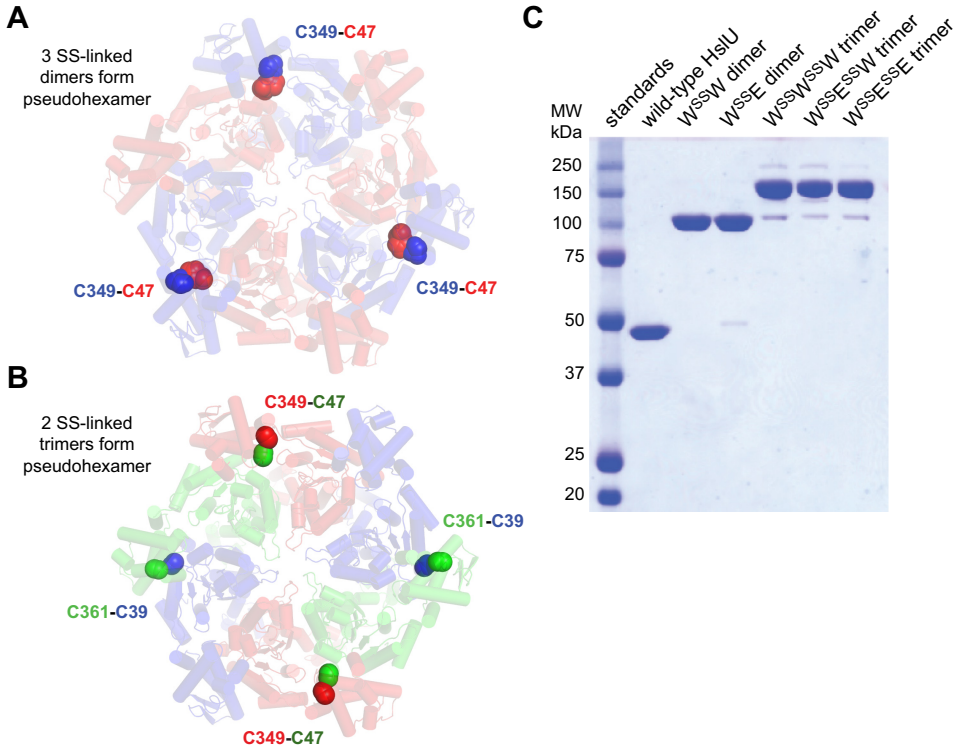

Figure 3. Design and purification of disulfide-cross-linked HslU variants. *A*, *spheres* show the positions of Cys^{47} (normally Glu) in *red* subunits and Cys^{349} (normally Ala) in *blue* subunits of an HslU hexamer, suggesting that Cys^{47}-Cys^{349} disulfides would stabilize a pseudohexamer consisting of three linked dimers. *B*, *spheres* show the positions of Cys^{349} in *red* subunits, Cys^{47} and Cys^{361} (normally Thr) in *green* subunits, and Cys^{39} (normally Gln) in *blue* subunits. Disulfide bond formation in this configuration would stabilize a pseudohexamer consisting of two linked trimers. *C*, non-reducing SDS-PAGE of purified wild-type HslU, purified $W^{SS}W$, purified $W^{SS}E$, purified $W^{SS}W^{SS}W$, purified $W^{SS}E^{SS}W$, and purified $W^{SS}E^{SS}E$. In each case, a 0.5 μM concentration of the purified protein (in hexamer equivalents) was loaded on the gel. The *first lane* contains molecular weight standards.

(19). For example, following purification by Ni^{2+}-NTA[5] affinity chromatography, non-reducing SDS-PAGE showed ~50% formation of $W^{SS}W$ and $W^{SS}E$ and ~33% formation of $W^{SS}W^{SS}W$, $W^{SS}E^{SS}W$, and $W^{SS}E^{SS}E$ (not shown). To further purify disulfide-linked pseudohexamers, we performed ion exchange chromatography and gel filtration chromatography once in the presence and once in the absence of urea, which destabilizes unlinked HslU hexamers more than linked hexamers. Following the final chromatography step, the $W^{SS}W$, $W^{SS}E$, $W^{SS}W^{SS}W$, $W^{SS}E^{SS}W$, and $W^{SS}E^{SS}E$ variants had purities of >95% (Fig. 3*C*). The disulfide-linked pseudohexamers bound HslV slightly more tightly than wild-type HslU (Table 2).

ATP hydrolysis by disulfide-linked pseudohexamers

Like the basal ATP hydrolysis activities of the genetically tethered pseudohexamers, those of the disulfide-linked enzymes were roughly proportional to the number of hydrolytically active W subunits in each pseudohexamer (Fig. 4, *A* and *B*). Compared with wild-type HslU, however, the $W^{SS}W_3$ and $W^{SS}W^{SS}W_2$ pseudohexamers were ~3-fold more hydrolytically active (Fig. 4*A*), possibly as a consequence of small conformational changes stabilized by the disulfide bonds. In the presence of HslV, the ATPase rate of wild-type HslU was stimulated ~3-fold, as observed previously (13, 20, 21), and ATP hydrolysis by $W^{SS}W_3$ and $W^{SS}W^{SS}W_2$ was stimulated ~2-fold, but ATP hydrolysis by $W^{SS}E_3$, $W^{SS}E^{SS}W_2$, or $W^{SS}E^{SS}E_2$ was not markedly stimulated (Fig. 4*C*). Thus, the presence of E subunits suppressed normal HslV stimulation of ATP hydrolysis by HslU pseudohexamers.

Degradation supported by disulfide-linked pseudohexamers

Arc repressor, a good substrate for HslUV degradation, is a metastable dimer that unfolds/dissociates with a half-life of ~10 s but refolds in milliseconds to maintain a predominantly native structure (15, 22). We assayed the ability of different disulfide-linked pseudohexamers to support HslV degradation of Arc-CysA, where CysA designates a unique cysteine labeled with an Alexa-488 fluorophore (23), as autoquenching of the fluorophores in the native protein is relieved upon degradation. The $W^{SS}W_3$ and $W^{SS}W^{SS}W_2$ pseudohexamers supported HslV degradation of a nearly saturating concentration of Arc-CysA at rates comparable with the wild-type HslU hexamer (Fig. 5*A*). Importantly, $W^{SS}E^{SS}W_2$ and $W^{SS}E_3$ also supported degradation at 35–45% of the wild-type rate, demonstrating that pseudohexamers with only three or four hydrolytically active subunits also have substantial degradation activity. Degradation supported by $W^{SS}E^{SS}E_2$ proceeded very slowly, at ~3% of the wild-type rate.

The degradation defects caused by E subunits in pseudohexamers were more severe for Arc-^{cp6}GFP-st11-ssrA, a stable substrate that wild-type HslUV degrades ~5-fold more slowly than Arc-CysA. $W^{SS}W_3$ and $W^{SS}W^{SS}W_2$ supported HslV deg-

[5] The abbreviations used are: NTA, nitrilotriacetic acid; BisTris, 2-[bis(2-hydroxyethyl)amino]-2-(hydroxymethyl)propane-1,3-diol; enz, enzyme concentration.

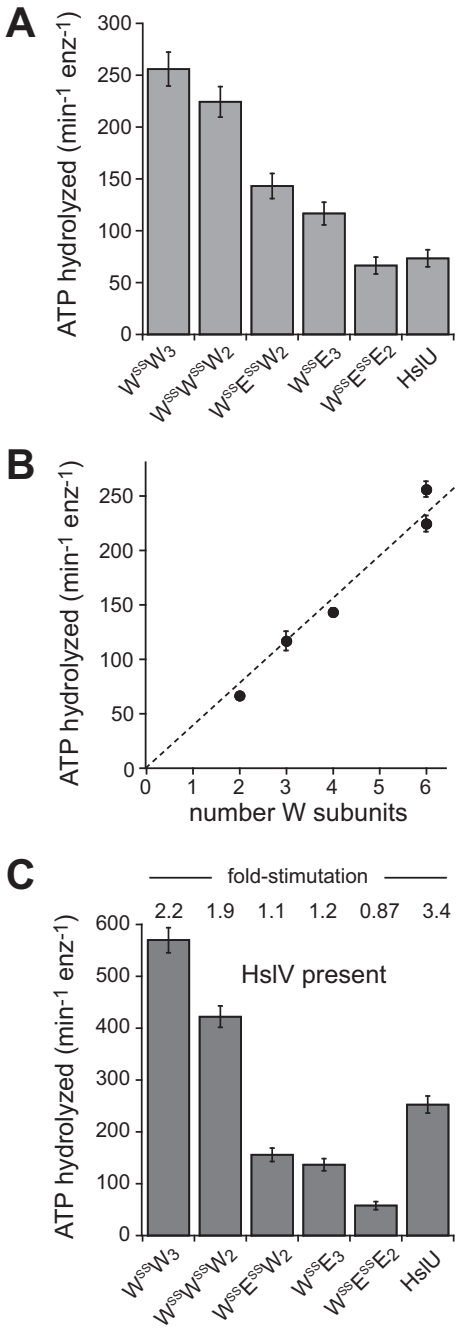

Figure 4. ATP hydrolysis by disulfide-cross-linked variants. *A*, basal rates of ATP hydrolysis by disulfide-cross-linked variants and wild-type HslU. Assays contained 0.3 μM HslU or pseudohexamers and 5 mM ATP. Values are averages of at least three replicates ± 1 S.D. (*error bars*). *B*, basal ATP hydrolysis rates for disulfide-cross-linked pseudohexamers plotted as a function of the number of W subunits. *C*, rates of ATP hydrolysis determined in the presence of 0.9 μM HslV dodecamer (other conditions as in *A*). The *numbers above* each *bar* represent the rate in the presence of HslV divided by the rate in the absence of HslV.

radation of a high concentration of Arc-^{cp6}GFP-st11-ssrA at nearly wild-type rates, but $W^{SS}E^{SS}W_2$ had only ~20% activity, $W^{SS}E_3$ had only ~10% activity, and $W^{SS}E^{SS}E_2$ was inactive (Fig. 5*B*). Degradation rates were normalized by dividing by the number of wild-type subunits in HslU or different variants and are plotted in Fig. 5*C* for the Arc-CysA substrate and Fig. 5*D* for the Arc-^{cp6}GFP-st11-ssrA substrate. For Arc-CysA, there was a sharp discontinuity between two and three wild-type subunits. For Arc-^{cp6}GFP-st11-ssrA, by contrast, the major discontinuity was between four and six subunits.

To determine the energetic efficiency of degradation of Arc-^{cp6}GFP-st11-ssrA, we assayed the rate of ATP-hydrolysis for each disulfide-linked pseudohexamer in the presence of HslV and Arc-^{cp6}GFP-st11-ssrA (Fig. 5*E*). We then divided the ATPase rate by the degradation rate to determine the average number of ATPs hydrolyzed during degradation of a single substrate (Fig. 5*F*). Notably, $W^{SS}W_3$, $W^{SS}E_3$, $W^{SS}W^{SS}W_2$, and $W^{SS}E^{SS}W_2$ all had similar energetic efficiencies, hydrolyzing ~500 ± 100 ATPs for each substrate degraded. Assuming that power strokes are tightly coupled to ATP hydrolysis, this result suggests that the $W^{SS}E^{SS}W_2$ and $W^{SS}E_3$ pseudohexamers use approximately the same number of power strokes as hexamers with six wild-type subunits to unfold and translocate Arc-^{cp6}GFP-st11-ssrA. Thus, the slower degradation activities of the $W^{SS}E^{SS}W_2$ and $W^{SS}E_3$ enzymes compared with pseudohexamers with only wild-type subunits are principally a consequence of their slower rates of ATP hydrolysis.

Discussion

Our studies show that *E. coli* HslU variants containing hydrolytically active and inactive subunits at specific positions in the hexameric AAA+ ring can hydrolyze ATP, unfold proteins, and degrade substrates in collaboration with HslV. As we discuss below, these results support a probabilistic model of ATP hydrolysis and provide insights into the multivalent interactions between HslU and HslV that are required for efficient protein degradation.

Genetic tethering allowed us to express and purify HslU pseudohexamers consisting of a trimer of linked dimers. However, the W-W_3 enzyme binds HslV poorly, suggesting that the tether interferes with HslV binding. Consistently, disulfide-linked pseudohexamers bind HslV well. In crystal structures of HslU hexamers alone, the C-terminal tails dock into a pocket, and the α-carboxyl group forms a salt bridge with an arginine in the sensor-2 motif of the same subunit (6, 10). These tail interactions were disrupted in several subunits in our low-resolution structure of W-E_3 pseudohexamers, as expected if the attached tether prevents proper packing of these residues. In the *H. influenzae* HslUV complex, the C-terminal tails are detached from HslU and pack into grooves on HslV, with the HslU α-carboxylate forming a salt bridge with an HslV lysine side chain (7, 11, 12). In *E. coli* HslUV structures, by contrast, the tails remain docked into HslU (8, 9). Moreover, deletion of the five C-terminal residues of *E. coli* HslU does not prevent stimulation of HslV peptidase activity or degradation (20). Nevertheless, peptides corresponding to the C-terminal residues of HslU activate peptide cleavage by *E. coli* HslV, and mutations in HslV predicted to disrupt contacts with the C-terminal tails prevent HslU activation (20, 24). Our results support the importance of the C-terminal tails in high-affinity HslV binding and indicate that more than three tails of *E. coli* HslU must interact optimally with HslV to allow tight binding and efficient proteolysis.

The pseudohexamers that we studied have basal ATP hydrolysis rates roughly proportional to their total number of hydrolytically active W subunits. This result supports a model in which the W subunits in these pseudohexamers contribute

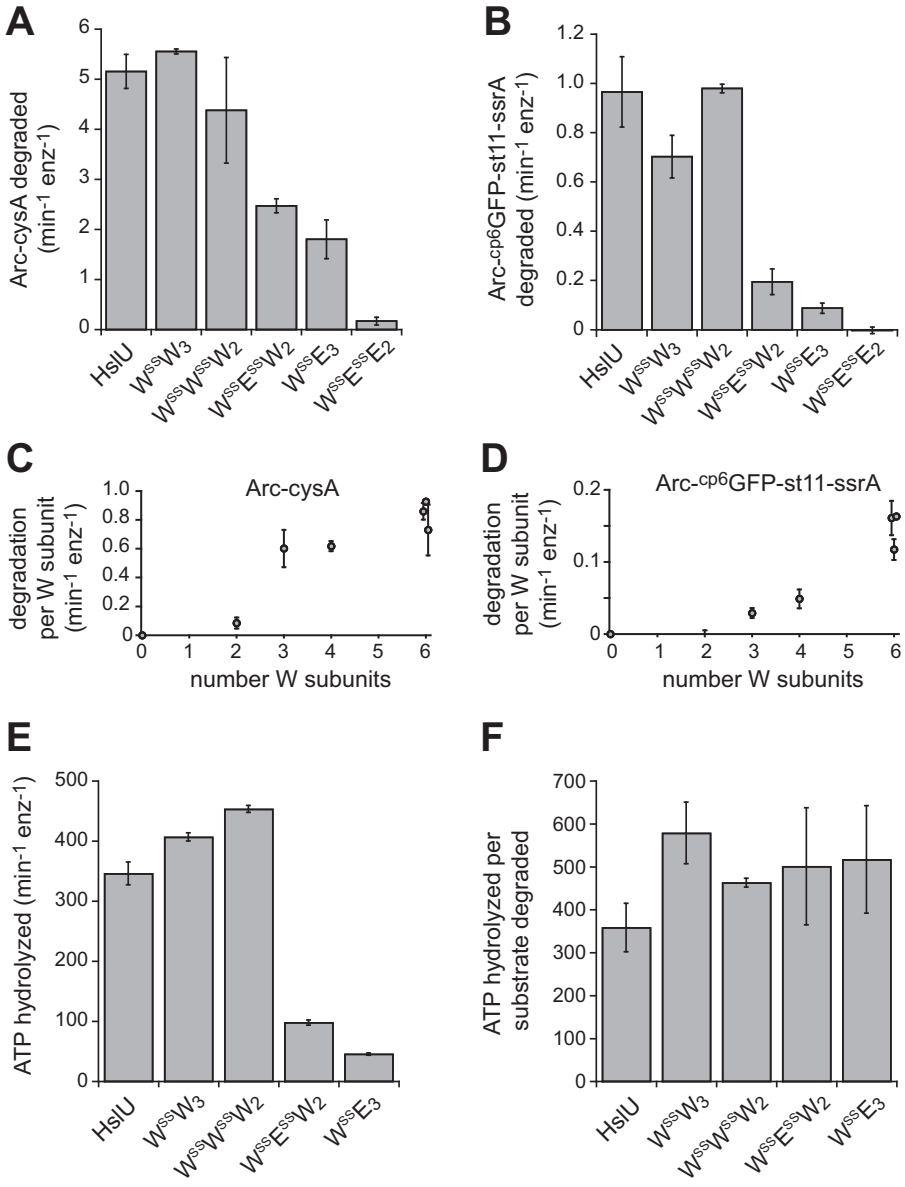

Figure 5. Degradation rates and energetic efficiencies of disulfide-cross-linked variants. *A*, rates of degradation of Arc-CysA (30 μM) assayed by increased fluorescence. *B*, rates of degradation of Arc-^{cp6}GFP-st11-ssrA (20 μM) assayed by decreased fluorescence. *C*, degradation rates for Arc-CysA from *A* were divided by the number of wild-type subunits in the HslU variant and plotted against this number. *D*, degradation rates for Arc-^{cp6}GFP-st11-ssrA from *B* were divided by the number of wild-type subunits in the HslU variant and plotted against this number. *E*, rates of ATP hydrolysis in the presence of 20 μM Arc-^{cp6}GFP-st11-ssrA and 1 μM HslV. *F*, energetic efficiency determined by dividing the ATPase rates by the degradation rates. For *A–D*, experiments were performed using 0.3 μM HslU or variants and 0.9 μM HslV. For *E* and *F*, experiments were performed using 0.5 μM HslU or variants and 1 μM HslV. All assays contained 5 mM ATP and were performed at 37 °C. Values in *A–E* are averages ($n \geq 3$) ± 1 S.D. (*error bars*). *Error bars* in *F*, propagated errors. In *C* and *D*, values for the three variants with six wild-type subunits were offset slightly on the *x* axis to allow visualization of *error bars*.

independently to basal ATPase activity, making concerted or strictly sequential models unlikely. For example, if ATP hydrolysis in a specific subunit required prior hydrolysis in a neighboring subunit, as expected in a strictly sequential model, then a non-linear relationship between W subunits and ATP hydrolysis would be expected. HslV stimulates ATP hydrolysis by $W^{SS}W_3$ and $W^{SS}W^{SS}W_2$ but caused little change in hydrolysis by $W^{SS}E^{SS}W_2$, $W^{SS}E_3$, or $W^{SS}E^{SS}E_2$. Because the E subunits in these latter enzymes also increase pseudohexamer affinity for HslV, stronger interactions between E subunits and HslV might restrict HslV-induced conformational changes required for higher ATPase activity in neighboring W subunits and thus explain the lack of ATPase stimulation. Alternatively, HslV binding might slow ATP dissociation from inactive E subunits, which becomes rate-limiting for hydrolysis in W subunits, especially if only a subset of subunits is nucleotide-bound at any given time.

Our strategies for engineering HslU rings with defined mixtures of active and inactive subunits were motivated by prior studies that applied these subunit-cross-linking methods to different hexameric AAA+ unfoldases and remodeling machines (5, 25–27). Indeed, genetic tethering experiments originally showed that ClpX also operates by a probabilistic mechanism, because ClpX pseudohexamers containing different combinations of hydrolytically active and inactive subunits unfold and degrade protein substrates in collaboration with the ClpP protease (5). Before the current study, however, it was not obvious

that HslU and ClpX would operate using similar probabilistic mechanisms of ATP hydrolysis. First, HslU and ClpX contain unique family-specific auxiliary domains. The I domain of HslU emerges from the top of the AAA+ ring, between the Walker A and Walker B ATPase motifs, and regulates ATP hydrolysis, degradation, and autoinhibition (9, 20, 23). The N domain of ClpX, by contrast, serves as a docking site for some adaptors/substrates, but its deletion has little effect on ATP hydrolysis or degradation of many ClpXP substrates (28). Second, in crystal structures, the large and small AAA+ domains of each HslU subunit assume orientations that create a potential nucleotide binding site, whereas the corresponding domains of ClpX adopt structures that allow nucleotide binding in some subunits but prevent binding in other subunits (6–12, 29). Third, HslU hexamers make symmetric interactions with hexameric rings of HslV, whereas ClpX hexamers make asymmetric interactions with heptameric rings of ClpP (30).

The tethered W-E_3 and E-W_3 HslU pseudohexamers have ~50% of the protein unfolding activity of the parental W-W_3 enzyme, and the disulfide-linked $W^{SS}E^{SS}W_2$ and $W^{SS}E_3$ enzymes support HslV degradation of an easily degraded Arc-CysA substrate at 35–45% of the parental rates. Thus, protein unfolding and translocation by the AAA+ ring of HslU do not require ATP hydrolysis in adjacent subunits or in subunits immediately across the ring from each other. Again, these results support a model in which probabilistic hydrolysis in the AAA+ ring powers unfolding and translocation. Slower rates of ATP hydrolysis in rings with mixtures of active and inactive subunits correlate with their reduced mechanical activities, because the ATP cost of degradation of the more stable Arc-^{cp6}GFP-st11-ssrA substrate is similar for the $W^{SS}E^{SS}W_2$ and $W^{SS}E_3$ pseudohexamers and their disulfide-linked parental enzymes containing six W subunits. Although optimal rates of ATP hydrolysis, unfolding, and degradation require six hydrolytically active HslU subunits, rings with only three or four active subunits use approximately the same number of power strokes to degrade this substrate.

We note that the $W^{SS}E^{SS}E_2$ pseudohexamer hydrolyzes ATP at ~40–60% of the $W^{SS}E_3$ rate but supports no degradation of Arc-^{cp6}GFP-st11-ssrA. These results suggest that some subunit-subunit communication is required for efficient unfolding and degradation by $W^{SS}E^{SS}E_2$ and/or that a minimum rate of ATP hydrolysis is required to unfold Arc-^{cp6}GFP-st11-ssrA. Probabilistic models of ATP hydrolysis do not exclude coordination between ring subunits for efficient ATP hydrolysis, substrate binding, or mechanical function. In fact, the rate of ATP hydrolysis and the degree of substrate binding by HslU change in a positively cooperative fashion with ATP concentration, as expected for functional linkage between different subunits (13). In the AAA+ ring of ClpX, communication between subunits is necessary to allow staged ATP binding to drive conformational changes needed for function (31–33). Moreover, optical trapping experiments reveal that kinetic bursts of power strokes in the ClpX ring result in random patterns of shorter and longer translocation steps, supporting a probabilistic but coordinated mechanism (34, 35). Similar themes of probabilistic hydrolysis but coordinated function are seen in AAA+ unfolding rings assembled from non-identical subunits. In the Yta10/Yta12 *m*-AAA protease, for example, mutating the Walker A motif of either the Yta10 or the Yta12 subunits does not affect hydrolysis in the remaining wild-type subunits, but Walker B mutations in Yta12 trap ATP and prevent robust hydrolysis in adjacent Yta10 subunits (36). Finally, in the six distinct subunits of the Rpt_{1-6} AAA+ ring of the 26S proteasome, Walker B mutations in individual subunits have a wide range of effects on ATP hydrolysis and mechanical activity, requiring a model with some subunit-subunit coordination within the context of an inherently probabilistic mechanism of ATP hydrolysis (37).

Experimental procedures

Cloning, expression, and protein purification

Mutants were constructed and cloned by standard PCR techniques unless otherwise noted. To construct genetically linked HslU dimers, a gene encoding two HslU subunits separated by the 20-residue ASGAGGSEGGGSEGGTSGAT linker was cloned into the pet11a vector (Novagen). HslU mutants used to make disulfide-cross-linked pseudohexamers were constructed in the cysteine-free $^{C262A/C288S}$HslU background with or without the E257Q mutation. Cysteine-free HslU supports robust ATP hydrolysis and substrate degradation (38–40). To make disulfide-cross-linked dimers, a gene encoding untagged ^{E47C}HslU was cloned into the first multiple cloning site (MCS1) of the pCOLADuet-1 (Novagen) vector between the NcoI and BamHI sites and a gene encoding His_6-ENLYFQS-^{A349C}HslU was cloned into MCS2 between the NdeI and XhoI sites, where His_6 is the hexahistidine tag and ENLYFQS is the sequence recognized and cleaved by the tobacco etch virus protease. ^{E47C}HslU had a glycine residue inserted after the initiator methionine as a result of cloning. This pCOLADuet-1 vector was transformed into the of *E. coli* SHuffle T_7 Express strain (New England Biolabs) for expression. To make disulfide-cross-linked trimers, a gene encoding untagged ^{A349C}HslU was cloned into MCS1 of pCOLADuet-1 between the NcoI and BamHI sites, and a gene encoding His_6-ENLYFQS-^{E47CT361C}HslU was cloned into MCS2 between the NdeI and XhoI sites. This vector was co-transformed with a pet12b (Novagen) vector encoding the untagged ^{Q39C}HslU variant into the SHuffle T_7 Express strain. Both ^{A349C}HslU and ^{Q39C}HslU contained an additional glycine after the initiator methionine as a result of cloning. A gene encoding the Arc repressor from phage P22 followed by a cysteine residue and a hexahistidine tag (Arc-Cys-His_6) was cloned and expressed in a pet21b vector (Novagen). Wild-type HslU and HslV were expressed from pet12b vectors. Arc-^{cp6}GFP-st11-ssrA and ^{I37A}Arc-^{cp6}GFP-β5/β6-st11-ssrA (in which a GGTEGSLVPRGSGESGGS sequence between β-stands 5 and 6 allows thrombin cleavage and generation of a split substrate), and Arc-st11-ssrA were expressed from pet21b vectors as described (14, 15, 23).

Genetically linked HslU dimers were expressed and purified as described previously for wild-type HslU (20). Disulfide-cross-linked HslU dimers were expressed and purified as follows. *E. coli* SHuffle T_7 Express cells carrying the pCOLADuet1 vector coding for the appropriate HslU mutants were grown at 30 °C until A_{600} of 0.6–0.8, the temperature was shifted to 18 °C, and protein expression was induced with 0.5

mM isopropyl 1-thio-β-D-galactopyranoside for 20 h. Cells were pelleted and resuspended in buffer A (50 mM Tris, pH 7.5, 300 mM NaCl, 20 mM imidazole, 0.5 mM EDTA), and 0.5 tablets of Complete Ultra EDTA-free protease inhibitor mixture (Roche Applied Science) and 1.5 μl of benzonase (250 units/μl; Sigma) per liter of the original culture were added. Cells were sonicated, the lysate was cleared by centrifugation, and 0.1% (v/v) PEI was added to the supernatant. This precipitate was cleared by centrifugation, and the supernatant was loaded onto Ni^{2+}-NTA beads equilibrated in buffer B (50 mM Tris, pH 7.5, 300 mM NaCl, 20 mM imidazole). The Ni^{2+}-NTA beads were washed extensively with buffer B, and protein was eluted with buffer C (50 mM Tris, pH 7.5, 300 mM NaCl, 250 mM imidazole). The eluate was diluted 3-fold with buffer D (50 mM Tris, pH 7.5, 10% (v/v) glycerol, 1 mM EDTA), loaded onto a Mono Q 10/100 GL column (GE Healthcare), and eluted with a linear gradient from 150 to 500 mM NaCl in buffer D (120 ml total). Appropriate Mono Q fractions were pooled, concentrated using an Amicon Ultra-15 centrifugal filter unit, and chromatographed on a Superdex 200 16/60 column (GE Healthcare) equilibrated in buffer E (50 mM Tris, pH 7.5, 300 mM NaCl, 10% (v/v) glycerol, 1.5 M urea, 1 mM EDTA), and 1-ml fractions were collected. Fractions with the highest purity of the cross-linked dimer as judged by non-reducing SDS-PAGE were pooled, concentrated, and run on another Superdex 200 16/60 column equilibrated in buffer F (50 mM Tris, pH 7.5, 300 mM NaCl, 10% (v/v) glycerol, 1 mM EDTA). Fractions with the highest purity of cross-linked dimer were pooled and concentrated. The concentration of cross-linked dimer was determined in hexameric equivalents by measuring the absorbance at 280 nm using 148,545 M^{-1} cm^{-1} as the molar extinction coefficient. Concentrated protein was divided into small aliquots and was flash-frozen at −80 °C.

Disulfide-cross-linked HslU trimers were expressed and purified largely as described for cross-linked dimers. His_6 tags were present on Cys^{349} subunits for dimers and Cys^{47}/Cys^{361} subunits for trimers. After precipitation with PEI, the sample was cleared by centrifugation, and the supernatant was loaded onto a 5-ml HisTrap HP column (GE Healthcare) equilibrated in buffer B. The column was washed with 75 ml of buffer B, the sample was eluted with a gradient of 20–500 mM imidazole in buffer B (100 ml total), and 2-ml fractions were collected. Fractions were pooled and dialyzed overnight against buffer G (50 mM Tris, pH 7.5, 150 mM NaCl, 10% glycerol (v/v), 1 mM EDTA) at 4 °C. The dialyzed material was loaded onto a Mono Q 10/100 GL column, and purification then proceeded by the method described for cross-linked dimers. The concentration of the cross-linked trimer was determined in hexameric equivalents by measuring absorbance at 280 nm using 147,180 M^{-1} cm^{-1} as the molar extinction coefficient. Concentrated protein was aliquoted and flash-frozen at −80 °C.

A pet21b vector carrying Arc with a C-terminal CHHHHHH tail (Arc-Cys-His_6) was transformed into the *E. coli* X90 (λDE3) *sly*D::*kan hsl*UV::*tet* strain, and cells were grown to an A_{600} of 0.6–0.8 at 37 °C. Protein expression was induced by the addition of 1 mM isopropyl 1-thio-β-D-galactopyranoside and continued for 4 h at room temperature. Cells were resuspended and lysed, and Arc-Cys-His_6 was purified by Ni^{2+}-NTA affinity chromatography as described for purification of cross-linked HslU dimers. After Ni^{2+}-NTA purification, protein was concentrated and injected onto a Superdex 75 16/60 column (GE Healthcare) equilibrated in buffer H (50 mM Tris, pH 7.5, 300 mM NaCl, 10% glycerol (v/v), 1 mM EDTA, 2 mM DTT). Fractions containing the Arc protein were concentrated and flash-frozen at −80 °C. Arc-Cys-His_6 was labeled with the maleimide derivative of Alexa-488 (Thermo Fisher Scientific) to generate Arc-CysA (23). His_6-tagged wild type HslU, His_6-tagged HslV, ^{I37A}Arc-^{cp6}GFP-β5/β6-st11-ssrA, Arc-^{cp6}GFP-st11-ssrA, and Arc-st11-ssrA were expressed and purified as described (23).

Biochemical assays

Unless noted, assays were performed at 37 °C in PD buffer (25 mM HEPES, pH 7.5, 5 mM KCl, 10% glycerol (v/v), 20 mM $MgCl_2$, 0.032% Igepal CA-630). Hydrolysis of 5 mM ATP was measured using an NADH-coupled assay (41) by monitoring the loss of absorbance at 340 nm on a Spectramax M5 plate reader (Molecular Devices). Cleavage of ^{I37A}Arc-^{cp6}GFP-β5/β6-st11-ssrA with thrombin was performed as described (14). Rates of unfolding of different concentrations of thrombin-split ^{I37A}Arc-^{cp6}GFP-β5/β6-st11-ssrA were determined by changes in ^{cp6}GFP fluorescence (excitation, 467 nm; emission, 511 nm) in assays that contained 0.5 μM HslU or tethered variants and 5 mM ATP. Degradation of 30 μM Arc-CysA (monomer equivalents) was measured on a Spectramax M5 plate reader by monitoring the increase in fluorescence (excitation, 480 nm; emission, 520 nm). Degradation of 20 μM Arc-^{cp6}GFP-st11-ssrA (monomer equivalents) was measured by monitoring the decrease in GFP fluorescence on a Spectramax M5 plate reader (excitation, 467 nm; emission, 511 nm). Degradation reactions contained 5 mM ATP and a regeneration system consisting of 16 mM creatine phosphate and 10 μg/ml creatine kinase. HslV activation assays were performed at 25 °C in the presence of ATP as described (13, 23), and $K_{½}$ values were determined by fitting to a hyperbolic equation.

Crystallography

The W-E_3 pseudohexamer was crystallized by the hanging drop method using 100 mM BisTris (pH 5.8), 26% (w/v) PEG 3350, and 260 mM ammonium sulfate as the well solution. Molecular replacement using Phaser (42) was initially used to solve the structure using a 1HQY hexamer (17) as the search model. We then replaced each 1HQY subunit with a 5JI3 subunit (23) to improve geometry and used rigid body refinement of individual domains, refinement of one *B*-factor and TLS group per subunit, and very tightly constrained positional refinement with torsional NCS constraints in Phenix (43). Coot (44) was used for model building, and MolProbity (45) was used to assess the geometry of the model.

Author contributions—J. C. performed experiments with HslU subunits linked by genetically encoded tethers. A. R. N. designed the split substrate for unfolding experiments. S. E. G., R. A. G., and R. T. S. performed crystallographic experiments. V. B. performed all remaining experiments. V. B. and R. T. S. wrote the manuscript. V. B., J. C., S. E. G., A. R. N., R. A. G., T. A. B, and R. T. S. contributed to the design and interpretation of experiments and approved the final manuscript.

References

1. Ogura, T., and Wilkinson, A. J. (2001) AAA+ superfamily ATPases: common structure–diverse function. *Genes Cells* **6,** 575–597
2. Snider, J., Thibault, G., and Houry, W. A. (2008) The AAA+ superfamily of functionally diverse proteins. *Genome Biol.* **9,** 216
3. Gai, D., Zhao, R., Li, D., Finkielstein, C. V., and Chen, X. S. (2004) Mechanisms of conformational change for a replicative hexameric helicase of SV40 large tumor antigen. *Cell* **119,** 47–60
4. Enemark, E. J., and Joshua-Tor, L. (2006) Mechanism of DNA translocation in a replicative hexameric helicase. *Nature* **442,** 270–275
5. Martin, A., Baker, T. A., and Sauer, R. T. (2005) Rebuilt AAA+ motors reveal operating principles for ATP-fuelled machines. *Nature* **437,** 1115–1120
6. Bochtler, M., Hartmann, C., Song, H. K., Bourenkov, G. P., Bartunik, H. D., and Huber, R. (2000) The structures of HsIU and the ATP-dependent protease HsIU-HsIV. *Nature* **403,** 800–805
7. Sousa, M. C., Trame, C. B., Tsuruta, H., Wilbanks, S. M., Reddy, V. S., and McKay, D. B. (2000) Crystal and solution structures of an HslUV protease-chaperone complex. *Cell* **103,** 633–643
8. Wang, J., Song, J. J., Franklin, M. C., Kamtekar, S., Im, Y. J., Rho, S. H., Seong, I. S., Lee, C. S., Chung, C. H., and Eom, S. H. (2001) Crystal structures of the HslVU peptidase-ATPase complex reveal an ATP-dependent proteolysis mechanism. *Structure* **9,** 177–184
9. Song, H. K., Hartmann, C., Ramachandran, R., Bochtler, M., Behrendt, R., Moroder, L., and Huber, R. (2000) Mutational studies on HslU and its docking mode with HslV. *Proc. Natl. Acad. Sci. U.S.A.* **97,** 14103–14108
10. Trame, C. B., and McKay, D. B. (2001) Structure of *Haemophilus influenzae* HslU protein in crystals with one-dimensional disorder twinning. *Acta Crystallogr. D Biol. Crystallogr.* **57,** 1079–1090
11. Sousa, M. C., Kessler, B. M., Overkleeft, H. S., and McKay, D. B. (2002) Crystal structure of HslUV complexed with a vinyl sulfone inhibitor: corroboration of a proposed mechanism of allosteric activation of HslV by HslU. *J. Mol. Biol.* **318,** 779–785
12. Kwon, A. R., Kessler, B. M., Overkleeft, H. S., and McKay, D. B. (2003) Structure and reactivity of an asymmetric complex between HslV and I-domain deleted HslU, a prokaryotic homolog of the eukaryotic proteasome. *J. Mol. Biol.* **330,** 185–195
13. Yakamavich, J. A., Baker, T. A., and Sauer, R. T. (2008) Asymmetric nucleotide transactions of the HslUV protease. *J. Mol. Biol.* **380,** 946–957
14. Nager, A. R., Baker, T. A., and Sauer, R. T. (2011) Stepwise unfolding of a β barrel protein by the AAA+ ClpXP protease. *J. Mol. Biol.* **413,** 4–16
15. Burton, R. E., Baker, T. A., and Sauer, R. T. (2005) Nucleotide-dependent substrate recognition by the AAA+ HslUV protease. *Nat. Struct. Mol. Biol.* **12,** 245–251
16. Sundar, S., McGinness, K. E., Baker, T. A., and Sauer, R. T. (2010) Multiple sequence signals direct recognition and degradation of protein substrates by the AAA+ protease HslUV. *J. Mol. Biol.* **403,** 420–429
17. Wang, J., Song, J. J., Seong, I. S., Franklin, M. C., Kamtekar, S., Eom, S. H., and Chung, C. H. (2001) Nucleotide-dependent conformational changes in a protease-associated ATPase HslU. *Structure* **9,** 1107–1116
18. Dombkowski, A. A. (2003) Disulfide by Design^{TM}: a computational method for the rational design of disulfide bonds in proteins. *Bioinformatics* **19,** 1852–1853
19. Lobstein, J., Emrich, C. A., Jeans, C., Faulkner, M., Riggs, P., and Berkmen, M. (2012) SHuffle, a novel *Escherichia coli* protein expression strain capable of correctly folding disulfide bonded proteins in its cytoplasm. *Microb. Cell Fact.* **11,** 56
20. Seong, I. S., Kang, M. S., Choi, M. K., Lee, J. W., Koh, O. J., Wang, J., Eom, S. H., and Chung, C. H. (2002) The C-terminal tails of HslU ATPase act as a molecular switch for activation of HslV peptidase. *J. Biol. Chem.* **277,** 25976–25982
21. Sundar, S., Baker, T. A., and Sauer, R. T. (2012) The I domain of the AAA+ HslUV protease coordinates substrate binding, ATP hydrolysis, and protein degradation. *Protein Sci.* **21,** 188–198
22. Milla, M. E., and Sauer, R. T. (1994) P22 Arc repressor: folding kinetics of a single-domain, dimeric protein. *Biochemistry* **33,** 1125–1133
23. Baytshtok, V., Fei, X., Grant, R. A., Baker, T. A., and Sauer, R. T. (2016) A structurally dynamic region of the HslU intermediate domain controls protein degradation and ATP hydrolysis. *Structure* **24,** 1766–1777
24. Ramachandran, R., Hartmann, C., Song, H. K., Huber, R., and Bochtler, M. (2002) Functional interactions of HslV (ClpQ) with the ATPase HslU (ClpY). *Proc. Natl. Acad. Sci. U.S.A.* **99,** 7396–7401
25. Glynn, S. E., Nager, A. R., Baker, T. A., and Sauer, R. T. (2012) Dynamic and static components power unfolding in topologically closed rings of a AAA+ proteolytic machine. *Nat. Struct. Mol. Biol.* **19,** 616–622
26. Biter, A. B., Lee, S., Sung, N., and Tsai, F. T. F. (2012) Structural basis for intersubunit signaling in a protein disaggregating machine. *Proc. Natl. Acad. Sci. U.S.A.* **109,** 12515–12520
27. Yamasaki, T., Oohata, Y., Nakamura, T., and Watanabe, Y. H. (2015) Analysis of the cooperative ATPase cycle of the AAA+ chaperone ClpB from *Thermus thermophilus* by using ordered heterohexamers with an alternating subunit arrangement. *J. Biol. Chem.* **290,** 9789–9800
28. Baker, T. A., and Sauer, R. T. (2012) ClpXP, an ATP-powered unfolding and protein-degradation machine. *Biochim. Biophys. Acta* **1823,** 15–28
29. Glynn, S. E., Martin, A., Nager, A. R., Baker, T. A., and Sauer, R. T. (2009) Structures of asymmetric ClpX hexamers reveal nucleotide-dependent motions in a AAA+ protein-unfolding machine. *Cell* **139,** 744–756
30. Grimaud, R., Kessel, M., Beuron, F., Steven, A. C., and Maurizi, M. R. (1998) Enzymatic and structural similarities between the *Escherichia coli* ATP-dependent proteases, ClpXP and ClpAP. *J. Biol. Chem.* **273,** 12476–12481
31. Stinson, B. M., Nager, A. R., Glynn, S. E., Schmitz, K. R., Baker, T. A., and Sauer, R. T. (2013) Nucleotide binding and conformational switching in the hexameric ring of a AAA+ machine. *Cell* **153,** 628–639
32. Hersch, G. L., Burton, R. E., Bolon, D. N., Baker, T. A., and Sauer, R. T. (2005) Asymmetric interactions of ATP with the AAA+ $ClpX_6$ unfoldase: allosteric control of a protein machine. *Cell* **121,** 1017–1027
33. Stinson, B. M., Baytshtok, V., Schmitz, K. R., Baker, T. A., and Sauer, R. T. (2015) Subunit asymmetry and roles of conformational switching in the hexameric AAA+ ring of ClpX. *Nat. Struct. Mol. Biol.* **22,** 411–416
34. Sen, M., Maillard, R. A., Nyquist, K., Rodriguez-Aliaga, P., Pressé, S., Martin, A., and Bustamante, C. (2013) The ClpXP protease unfolds substrates using a constant rate of pulling but different gears. *Cell* **155,** 636–646
35. Cordova, J. C., Olivares, A. O., Shin, Y., Stinson, B. M., Calmat, S., Schmitz, K. R., Aubin-Tam, M.-E. Baker, T. A., Lang, M. J., and Sauer, R. T. (2014) Stochastic but highly coordinated protein unfolding and translocation by the ClpXP proteolytic machine. *Cell* **158,** 647–658
36. Augustin, S., Gerdes, F., Lee, S., Tsai, F. T., Langer, T., and Tatsuta, T. (2009) An intersubunit signaling network coordinates ATP hydrolysis by m-AAA proteases. *Mol. Cell* **35,** 574–585
37. Beckwith, R., Estrin, E., Worden, E. J., and Martin, A. (2013) Reconstitution of the 26S proteasome reveals functional asymmetries in its AAA+ unfoldase. *Nat. Struct. Mol. Biol.* **20,** 1164–1172
38. Yoo, S. J., Kim, H. H., Shin, D. H., Lee, C. S., Seong, I. S., Seol, J. H., Shimbara, N., Tanaka, K., and Chung, C. H. (1998) Effects of the Cys mutations on structure and function of the ATP-dependent HslVU protease in *Escherichia coli.* The Cys^{287} to Val mutation in HslU uncouples the ATP-dependent proteolysis by HslVU from ATP hydrolysis. *J. Biol. Chem.* **273,** 22929–22935
39. Seong, I. S., Oh, J. Y., Yoo, S. J., Seol, J. H., and Chung, C. H. (1999) ATP-dependent degradation of SulA, a cell division inhibitor, by the HslVU protease in *Escherichia coli*. *FEBS Lett.* **456,** 211–214
40. Yakamavich, J. A. (2008) *Control of HslUV Protease Function by Nucleotide Binding and Hydrolysis*, Ph.D. thesis, Massachusetts Institute of Technology, Cambridge, MA
41. Nørby, J. G. (1988) Coupled assay of Na^+,K^+-ATPase activity. *Methods Enzymol.* **156,** 116–119
42. McCoy, A. J., Grosse-Kunstleve, R. W., Adams, P. D., Winn, M. D., Storoni, L. C., and Read, R. J. (2007) Phaser crystallographic software. *J. Appl. Crystallogr.* **40,** 658–674

43. Adams, P. D., Afonine, P. V., Bunkóczi, G., Chen, V. B., Davis, I. W., Echols, N., Headd, J. J., Hung, L. W., Kapral, G. J., Grosse-Kunstleve, R. W., McCoy, A. J., Moriarty, N. W., Oeffner, R., Read, R. J., Richardson, D. C., *et al.* (2010) PHENIX: a comprehensive Python-based system for macromolecular structure solution. *Acta Crystallogr. D Biol. Crystallogr.* **66,** 213–221
44. Emsley, P., Lohkamp, B., Scott, W. G., and Cowtan, K. (2010) Features and development of Coot. *Acta Crystallogr. D Biol. Crystallogr.* **66,** 486–501
45. Chen, V. B., Arendall, W. B., 3rd, Headd, J. J., Keedy, D. A., Immormino, R. M., Kapral, G. J., Murray, L. W., Richardson, J. S., and Richardson, D. C. (2010) MolProbity: all-atom structure validation for macromolecular crystallography. *Acta Crystallogr. D Biol. Crystallogr.* **66,** 12–21